CALPHAD: Computer Coupling of Phase Diagrams and Thermochemistry 68 (2020) 101731

Contents lists available at ScienceDirect

Calphad

journal homepage: http://www.elsevier.com/locate/calphad

Impact of magnetism on the phase stability of rare-earth based hard magnetic materials

Halil İbrahim Sözen *, Tilmann Hickel, Jörg Neugebauer

Max-Planck-Institut für Eisenforschung GmbH, Max-Planck-Str. 1, 40237, Düsseldorf, Germany

ARTICLE INFO

Keywords:
Phase stabilities
Inden model
ab initio thermodynamics
Ce-based hard magnets
Magnetic models

ABSTRACT

In recent years, quantum-mechanically guided materials design has been used to identify candidate hard magnetic materials with a reduced content of rare earth elements. The focus of these studies was on optimal magnetic properties. In the present work we address the issue of thermodynamic stability of such materials. As prototype system we consider $CeFe_{11}Ti$ and focus on the impact of magnetism on the free energy. To this end, we use the magnetic model suggested by Gerhard Inden as a reference. The performance of this model is compared to Monte Carlo simulations for the magnetic entropy contribution. We conclude that despite the empirical nature of the Inden model, it provides a surprisingly accurate description of the magnetic contribution. Based on this approach we are able to faithfully predict the critical temperature for the decomposition of $CeFe_{11}Ti$ into competing Laves phases. We further show that the Inden model can be improved if the reduction of the magnetic moment at finite temperatures is taken into account. This is demonstrated for the hard magnetic phase $Nd_2Fe_{14}B$. In addition, the impact of magnetism on the lattice vibrations of relevant phases in the Ce–Fe–Ti system is analyzed.

1. Introduction

Permanent magnets are critical components in various electronic devices. Applications range from generators of wind turbines to speakers of smartphones [1]. Most of the currently applied hard magnetic materials contain rare-earth (RE) and transition metal (TM) elements. The desired magnetic properties such as a high magnetic energy density, a large magnetocrystalline anisotropy and a high Curie temperature have most convincingly been achieved by $Nd_2Fe_{14}B$ magnets [2,3]. A disadvantage of this alloy is the need of rare-earth additions that are limited and economically expensive.

Next to experimental efforts [4,5], theoretical approaches promise to design novel magnets that are free of these expensive constituents. To find compositions with comparable magnetic properties, high-throughput screening calculations have been performed [6,7]. At the same time, theoretical efforts on such RE based alloys have been made that focus on magnetic properties such as the 4*f*-electrons magnetism [8], site preferences of substituted RE elements and mixed valency treatments [9,10] and intrinsic magnetic properties [11]. These methodologies and efforts are aiming at ground state properties. So far, the question of the thermodynamic stability of the thus identified phases has not been addressed.

For the determination of phase stabilities, the calculation of the free energy for individual phases is vital. Next to Calphad, *ab initio* approaches have been successfully used for computing the phase stability of various nonmagnetic materials and have shown to provide accurate predictions [12,13]. In both approaches, however, integrating magnetic entropies is not straight forward but important for the description of the considered material. A pragmatic solution has been introduced by Chuang et al. [14]: empirical mathematical expressions are used to describe the heat capacity of several magnetic elements and binaries. Within the Calphad community a formulation suggested by Inden [15,16] is widely used and has been established as a reliable tool. Despite its simplicity, this method turned out to be highly successful in the accurate thermodynamic description of many material systems.

In order to assess the various empirical methods, we determine in this paper the magnetic free energy contribution by using the Heisenberg model with the Hamiltonian,

$$\mathscr{H} = \sum_{ij} J_{ij} \mathbf{S}_i \mathbf{S}_j. \quad (1)$$

Here, the spins $\mathbf{S}_{i(j)}$ are assumed to be localized at lattice sites *i* and *j*. The exchange interactions J_{ij} can be determined with different DFT methods such as the Korringa-Kohn-Rostoker (KKR) technique [17,18]

* Corresponding author.
E-mail address: h.soezen@mpie.de (H.İ. Sözen).

https://doi.org/10.1016/j.calphad.2019.101731
Received 7 October 2019; Received in revised form 11 December 2019; Accepted 16 December 2019
Available online 27 December 2019

or the application of the magnetic force theorem [19]. Although the exact analytical solution of the Hamiltonian in Eq. (1) is not known, classical Monte Carlo (cMC) [20] techniques can be used to provide a numerical solution for a given set of J parameters. In special cases, even quantum Monte Carlo (qMC) [21] simulations can be performed. Therefore, an *ab initio* determined set of J_{ij} energies gives access to several magnetic properties such as the total magnetization at finite temperatures and the magnetic heat capacity.

In this present work, we demonstrate the importance of including magnetism in modeling the thermodynamic stability of RE-based hard magnets. As shown in our recent work [22], $CeFe_{11}Ti$ is a promising candidate for novel hard magnetic applications. We therefore focus in this study on Ce–Fe–Ti alloys. The paper is organized as follows: In Sec. II we explain the technical aspects of our computational methods for *ab initio* thermodynamics and specially the treatment of magnetism. In Sec. III the impact of magnetism on phase stabilities and the methodological challenges in modeling RE-TM containing $CeFe_2$ binaries are given. Also a comparison between the *ab initio* approach and the Inden model for various alloys is presented. Sec. IV covers the impact of magnetism on the phonon dispersions of relevant Ce–Fe–Ti alloys. In Sec. V the performance of the Inden model is further tested for Ce and Nd-based magnetic materials. It also includes a sensitivity analysis for 3 different input parameters. We finally conclude the paper in Sec. VI.

2. Computational details

In this work, all first principles calculations are based on DFT as implemented in the Vienna *ab initio* simulation package VASP [23,24]. The projector-augmented wave (PAW) [25] method is employed. Exchange-correlation is treated within the generalized gradient approximation (GGA) of Perdew-Burke-Ernzerhof (PBE) [26]. In particular, the Ce potential with $5s^2 5p^6 4f^1 5d^1 6s^2$ valence configuration is selected, where the single f-electron is treated explicitly as valence state in DFT. To address the localized 4f-electrons in $Nd_2Fe_{14}B$ the DFT + U method proposed by Dudarev et al. [27] is employed. However, in the case of Ce-based binaries as well as the Ce–Fe–Ti ternary compound investigated here, a Hubbard U correction is not needed. The underlying reason for this is the strong hybridization of Ce-4f with TM-3d electrons, which gives rise to an earlier filling of the bonding bands compared to the localized 4f of Ce. We further refer to Ref. 22 for more technical details.

In order to calculate phase stabilities and thermodynamic properties, DFT is not only applied to ground state energies, but also used to determine finite temperature excitations [28]. The free energies are considered in the adiabatic approximation, therewith decoupling the degrees of freedom

$$F(T,V) = E_0(V) + F^{\mathrm{el}}(T,V) + F^{\mathrm{vib}}(T,V) + F^{\mathrm{mag}}(T,V), \tag{2}$$

which are the zero-temperature total energy E_0, the thermal electronic F^{el}, the vibrational F^{vib} and the magnetic F^{mag} contributions to the free energy.

The thermal electronic contribution to the free energy, F^{el}, is calculated by using the finite temperature formulation of DFT [29].

$$F^{\mathrm{el}} = E^{\mathrm{tot}}(T,V) - E_0(V) - TS^{\mathrm{el}}, \tag{3}$$

where E^{tot} is the total electronic free energy (including the binding energies at 0 K). S^{el} is the electronic entropy obtained from Fermi occupation numbers f_i

$$S^{\mathrm{el}} = k_{\mathrm{B}} \sum_i (f_i \ln f_i + (1-f_i)\ln(1-f_i)), \tag{4}$$

with k_{B} the Boltzmann constant. We note that the electronic contribution is evaluated for static lattice positions, though lattice vibrations modify the electronic density of states close to the melting point [30]. The evaluation of these coupling effects requires explicit *ab initio* molecular dynamics simulations, which is beyond the scope of the present manuscript.

Phonon spectra are computed with the *direct force constant method* [31,32] and used as an input for the vibrational free energy F^{vib} as well. A displacement of 0.02 Å is used for all phases to calculate Hellmann-Feyman forces. The number of inequivalent displacements depends on the symmetry of the crystal structure (translational and rotational symmetries) and the occupation of the sublattice. In order to determine these symmetries automatically we have used the S/PHI/nX tool [33,34]. The forces in a displaced structure are calculated using VASP. We have used the Methfessel-Paxton scheme [35] with a broadening parameter 0.1 eV. The k-point sampling is chosen such that F^{vib} is converged to ~1 meV/atom. For example, 10 × 10 × 10 k-points for a 3 × 3 × 3 (54 atoms) supercell of B2–FeTi have been used (that corresponds to 54 × 10^3 kp · atom). The convergence criterion for the electronic loop has been set to 10^{-6} eV. The eigenvalues of the Fourier transformed dynamical matrix ω_i enter the free energy expression in harmonic approximation [36].

$$F^{\mathrm{vib}} = \frac{1}{N} \sum_i^{3N} \left\{ \hbar\omega_i + k_{\mathrm{B}} T \ln\left[1 - \exp\left(-\frac{\hbar\omega_i}{k_{\mathrm{B}} T}\right)\right]\right\}, \tag{5}$$

where $\hbar$ is the reduced Planck constant. The summation in Eq. (5) runs over all 3 N phonon states, where N is the number of atoms in the unit cell. In the *quasi-harmonic approximation* considered here, the volume dependence of the phonon frequencies, ω_i, is additionally taken into account. Explicitly anharmonic contributions are not considered. In many magnetic materials, the phonon frequencies may depend on the actual magnetic state (see, e.g., Refs. [37, 38]). Therefore, this impact of magnetism will also be analyzed in the present work.

The emphasis is, however, on the magnetic free energy, F^{mag}, and its treatment with the empirical formula developed in a pioneering work by Gerhard Inden [15] in 1976. The magnetic part of the heat capacity C_{mag} has a different physical origin below and above the magnetic transition temperature T_C. At temperatures below T_C a long range order (LRO) of the magnetic degrees of freedom is present. Slightly above T_C the distribution of the local magnetic moment directions is not yet random, but a short range order (SRO) can still be observed. Inden demonstrated that both regions of the heat capacity can be mathematically described by very similar LRO and SRO models as

$$\begin{cases} C_P^{\mathrm{LRO}} = K^{\mathrm{LRO}} R \ln\dfrac{1+\tau^3}{1-\tau^3}, & \tau < 1 \\ C_P^{\mathrm{SRO}} = K^{\mathrm{SRO}} R \ln\dfrac{1+\tau^{-5}}{1-\tau^{-5}}, & \tau > 1 \end{cases} \tag{6}$$

where C_P^{LRO} and C_P^{SRO} designate the magnetic heat capacity in the ferromagnetic (FM) and paramagnetic (PM) states, R is the gas constant and τ is the normalized temperature T/T_C. The temperature independent empirical character is given in the LRO and SRO prefactors by

$$K^{\mathrm{SRO}} = \frac{0.784 \cdot f \cdot S^{\mathrm{mag}}/R}{0.5979 - 0.2114 f}, \tag{7}$$

$$K^{\mathrm{LRO}} = \frac{S^{\mathrm{mag}}/R - 0.493 K^{\mathrm{SRO}}}{0.822}. \tag{8}$$

These equations have two further parameters, which are the ratio between the magnetic enthalpy due to SRO and LRO, f and the magnetic entropy, S^{mag}. The magnetic enthalpy ratio is given by

$$f = \frac{\Delta H^{\mathrm{SRO}}(\infty)}{\Delta H^{\mathrm{SRO}}(\infty) + \Delta H^{\mathrm{LRO}}(T_C)}, \tag{9}$$

where the enthalpy change ΔH is obtained from the integration of the heat capacities given in Eq. (6). The f parameter is calculated by Inden to

be 0.4 for bcc Fe and 0.28 for fcc Co and Ni [15], which has been generalized as the choice for bcc and fcc ferromagnets, respectively. The maximum magnetic entropy of an element with fixed magnetic moment β is

$$S_{\max}^{\mathrm{mag}} = R\ln(\beta+1), \tag{10}$$

if β is in units of Bohr magneton.

Therefore, the Inden approach is using three physical parameters, which are the critical temperature T_C, the enthalpy ratio f, and the mean magnetic moment β. Since the Inden approach [15] was considered to be computationally too expensive for efficient calculations of phase diagrams, the logarithmic function has been approximated by Hillert an Jarl [39] in 1978

$$\begin{cases} C_P^{\mathrm{LRO}} = 2K^{\mathrm{LRO}}R\left(\tau^m + \frac{1}{3}\tau^{3m} + \frac{1}{5}\tau^{5m}\right), & \tau < 1 \\ C_P^{\mathrm{SRO}} = 2K^{\mathrm{SRO}}R\left(\tau^{-n} + \frac{1}{3}\tau^{-3n} + \frac{1}{5}\tau^{-5n}\right), & \tau > 1, \end{cases} \tag{11}$$

where $m = 3$ and $n = 5$. Being a power series expansion, the basic structure of the expression for the heat capacity given in Eq. (6) and of the set of parameters are unchanged. Since this expression does not yield a mathematical divergence at the transition temperature, it is commonly used in CALPHAD databases as a description of magnetism. Several other modifications exist, including the proposal of Chen and Sundman to extend the expansion to seventh order [40].

A critical parameter in the above formulation is the magnetic moment β, which is used to calculate the magnetic entropy and controls the magnitude of the λ-shaped magnetic heat capacity. In the case of multi-component alloys the simplest choice for β is the mean magnetic moment [16]. If the individual magnetic moments β_i are known, they can be weighted with their mole fraction x_i, yielding an effective magnetic moment [41] β via

$$S_{max}^{\mathrm{mag}} = R\ln(\beta+1) = R\sum_i x_i \ln(\beta_i+1). \tag{12}$$

Since the effective magnetic moments are supposed to give more accurate results than mean moments [41], this concept has been used in the present work. The magnetic moments, which were used as input parameters for Eq. (12), were calculated from *ab initio* and are listed in Table 1.

The resulting expression for the Gibbs energy using an additional term [40] and $n = 7$ in Eq. (11) is given as [41].

$$G^{\mathrm{mag}} = TS^{\mathrm{mag}}g(\tau), \tag{13}$$

$$g(\tau) = \begin{cases} 0 & \tau \le 0 \\ 1 - \frac{1}{D}\left[0.38438376\frac{\tau^{-1}}{f} + 0.63570895\left(\frac{1}{f}-1\right)\left(\frac{\tau^3}{6} + \frac{\tau^9}{135} + \frac{\tau^{15}}{600} + \frac{\tau^{21}}{1617}\right)\right] & 0 < \tau \le 1 \\ -\frac{1}{D}\left(\frac{\tau^{-7}}{21} + \frac{\tau^{-21}}{630} + \frac{\tau^{-35}}{2975} + \frac{\tau^{-49}}{8232}\right) & \tau > 1 \end{cases} \tag{14}$$

$$D = 0.33471979 + 0.49649686\left(\frac{1}{f}-1\right). \tag{15}$$

Here, the structural factor f is modified to 0.37 for bcc and 0.25 for non-bcc crystal structures, due to the re-optimized K^{SRO} and K^{LRO} values for the extension of the power series to seventh order. However, this change in f does not have a significant effect on the heat capacity for Co and Ni, as shown by Chen and Sundman [40].

Table 1
Calculated magnetic moments, M, for the considered element and alloys in the competition energy (Eq. (17)) by using first principles. The corresponding sub-lattices are given in parenthesis.

Phase	Magnetic moment M (μ_B)
Fe	2.21
Fe_2Ti	1.31 Fe (6*h*), 0 Fe (2*a*), 0.14 Ti (4*f*)
$CeFe_2$	1.81 Fe (16*a*), -0.91 Ce (8*b*)
$CeFe_{11}Ti$	2.30 Fe (8*i*), 1.76 Fe (8*f*), 2.18 Fe (8*j*), −0.74 Ce (2*a*), -1.07 Ti (8*i*)

One has to take into account that G^{mag} as given in Eq. (13) has been developed to describe the magnetic free energy arising from magnetic ordering. Therefore, the total magnetic free energy, F^{mag}, is the sum of this term and the free energy contribution of the paramagnetic disorder, which is considered by the expression

$$G_{\mathrm{mag}}^{\mathrm{PM}}(T) = \mathrm{R}T\ln(\beta+1). \tag{16}$$

We note that an alternative empirical expression has been employed recently to investigate the partitioning of substitutional impurities in cementite and ferrite by Sawada et al. [42]. They have calculated the heat capacity analytically as given by Chuang et al. [14].

3. Impact of magnetic models on phase stabilities

As mentioned above, the $CeFe_{11}Ti$ phase shows the most promising hard magnetic properties among the Ce–Fe–Ti alloys. However, the presence of Ti also yields the formation of the secondary Fe_2Ti Laves phase. Similarly, depending on its chemical potential, Ce can give rise to large phase fractions of $CeFe_2$ in the microstructure, which are detrimental for the magnetic performance of the material.

To computationally predict and subsequently suppress the stability of the Laves phases at elevated temperature, their temperature dependent free energies need to be determined by means of Eq. (2). The relative stability of $CeFe_{11}Ti$ with respective to a decomposition into the two Laves phases and pure α-Fe is given by the following expression [22].

$$F^{\mathrm{dec}}(T,V) = F^{\mathrm{CeFe_{11}Ti}}(T,V) - 7F^{\mathrm{Fe}}(T,V) - \left(F^{\mathrm{CeFe_2}}(T,V) + F^{\mathrm{Fe_2Ti}}(T,V)\right) \tag{17}$$

A positive value of F^{dec} means that the decomposition of $CeFe_{11}Ti$ into the three competing phases is favored, while the desired $CeFe_{11}Ti$ phase is stable for negative values. Here, all phases have been considered as line compounds, ignoring solubility regions in the common tangent construction. Furthermore, our previous analysis demonstrated that a consideration of additional binary phases in the phase diagram is not required [22].

The *ab initio* computed temperature dependence of F^{dec} is plotted in Fig. 1. Here, the main result is the red line, for which electronic, vibrational and magnetic entropy contributions are taken into account,

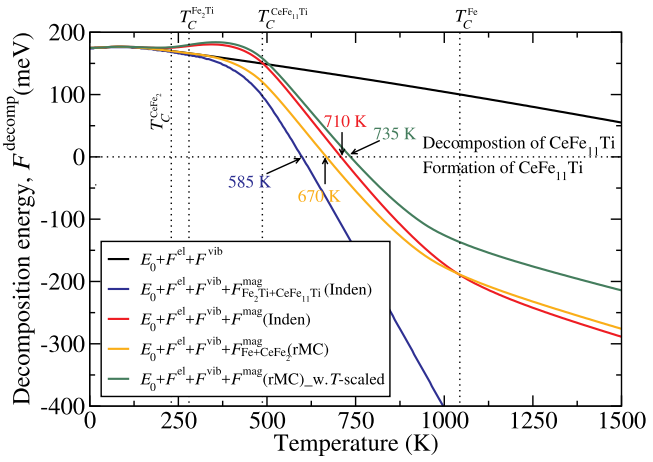

Fig. 1. Temperature dependence of the decomposition energy F^{dec}, which determines the phase stability of $CeFe_{11}Ti$. An approach with the full free energy, including the Inden model for the magnetic contribution F^{mag} (red line) is compared to a calculation without magnetic entropy (black line). Starting from the full result, the magnetic entropy of the phases Fe and $CeFe_2$ has been removed (blue line) and replaced by rescaled Monte Carlo simulations with (green line) and without (orange line) adjusted Curie temperatures.

the latter using the above described modified Inden model. The competition energy yields positive values up to 710 K, indicating a thermodynamic instability of $CeFe_{11}Ti$ due to the decomposition into $CeFe_2$, Fe_2Ti and Fe. Above this critical temperature, however, the ternary hard magnetic phase will form. This result has been published earlier [22] and the dependence of the stability on the annealing temperature is consistent with experiments using the reactive crucible melting (RCM) technique. The latter method indicates the presence of the $CeFe_{11}Ti$ phase above 1173 K and its absence at lower temperatures, but cannot provide exact decomposition temperatures due to kinetic limitations.

Since the focus of the present discussions is on the magnetic contribution, we have also plotted the decomposition energy without magnetic free energy contributions in Fig. 1 (black line). The result is remarkably different. Over the whole temperature range plotted here, F^{dec} now shows positive values, i.e. a decomposition of $CeFe_{11}Ti$ into $CeFe_2$, Fe_2Ti and Fe. This is clearly inconsistent with experiments, such as RCM, where the formation of the phase at latest sets in at 1173 K. This result demonstrates the importance of including magnetic contribution to accurately describe the temperature dependence of the phase stability. At the same time, it raises the question how severe the applied magnetic approximations are for this result.

To benchmark the magnetic results obtained with the Inden model, we have performed *ab initio* based Monte Carlo simulations. To limit the computational effort, the phases $CeFe_{11}Ti$ and Fe_2Ti are still treated with the Inden model, and only the impact of the magnetic entropy for the phases α-Fe and C15–$CeFe_2$ has been evaluated, both contributing to F^{dec} in Eq. (17).

Ignoring the magnetic entropy for the latter two phases yields the blue line in Fig. 1. One observes a substantially reduced critical temperature for decomposition (585 K) as compared to the full result (710 K). The main reason is the missing change of curvature at the Curie temperature of $CeFe_2$ (230 K). The magnetic entropy of Fe, however, is only significant for temperatures above 1000 K and therefore does not affect the critical temperature of decomposition. Furthermore, for Fe Monte Carlo calculations have been published earlier [43]. Therefore, we will focus in this study on the phase $CeFe_2$ only to discuss the challenges of an *ab initio* based magnetic modeling of RE-TM compounds. This will give sufficient insights into the reliability of the methods.

We have started with the calculation of the exchange-coupling parameters using the *ab initio* electronic structure code Machikaneyama

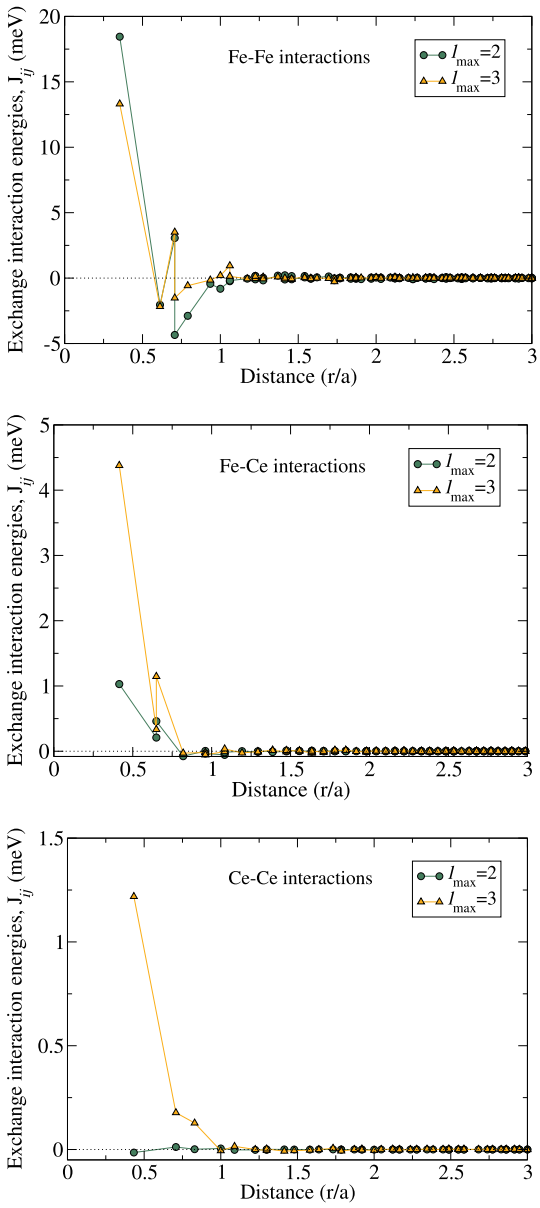

Fig. 2. Calculated exchange interaction energies for $CeFe_2$ as a function of distance. Two different treatments of the *f*-electrons are compared: for $l_{max} = 2$ the *f*-electrons are part of the core and for $l_{max} = 3$ they are considered as valence electrons. In all cases, experimental lattice constants are used.

(AkaiKKR) [44–46]. It employs the Korringa-Kohn-Rostoker Green's function method, following the prescription proposed by Lichtenstein et al. [47]. The calculated exchange interactions for $CeFe_2$ are given in Fig. 2. The two sublattices of C15–$CeFe_2$, namely Fe (16*a*) and Ce (8*b*), give rise to the three kinds of interactions Fe–Fe, Fe–Ce and Ce–Ce that are shown separately in the figure. Positive energies imply ferromagnetic and negative ones antiferromagnetic interactions.

The 4*f*-electrons are treated in two different ways. The setting $l_{max} = 3$ puts all the 4*f*-electrons in the valence state and $l_{max} = 2$ treats them in the core. The *f*-electrons in the valence mainly increase the nearest neighbor (NN) interactions for Fe–Ce and Ce–Ce (e.g., by almost 450% for Fe–Ce). There is also an indirect impact of the *f*-electrons on the Fe–Fe interactions, with a decrease of the NN interaction by ~25%. Substantial consequences are observed in the magnetic heat capacity, Fig. 3(a). For both cases, the transition temperature from the ordered to the disordered state appears at ~500 K, well above the experimental [48] transition temperature of 230 K. In case of the treatment with l_{max}

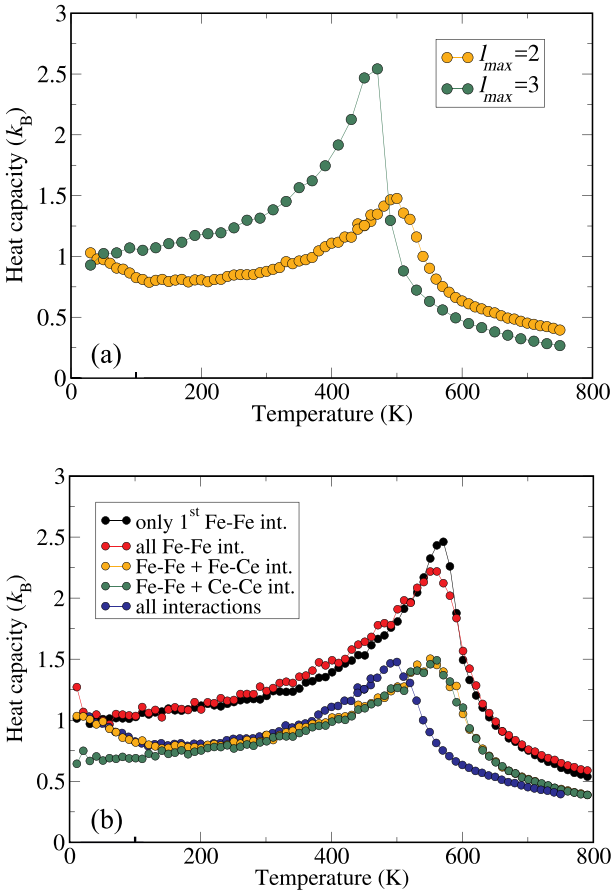

Fig. 3. Classical Monte Carlo calculations of the magnetic heat capacity of $CeFe_2$ for the two different treatments of the *f*-electrons shown in (a) and restricting the exchange interactions to certain pairs of atoms for $l_{max} = 2$ (b). The cMC calculations have been performed in $10 \times 10 \times 10$ supercells with the same lattice constants.

$= 3$, the λ-shaped peak is more pronounced and narrow than for $l_{max} = 2$. Further, the height and shape of the peak are more consistent with experiment [48], considering the overestimation by a classical as compared to a quantum-mechanical calculation.

Furthermore, Fig. 3 shows for $l_{max} = 2$ an unexpected minimum at ~200 K, which we have not observed in earlier classical MC calculations of Fe-based materials. We were able to demonstrate in Fig. 3(b) that this feature is due to the treatment of the 3*d*-4*f* interactions: It is not observed, if we limit ourselves to the 18 NN Fe–Fe interactions, which form the largest contribution to the heat capacity. The additional 864 Fe–Fe interactions in a range of 1.5 times the lattice constant hardly change the heat capacity. If Ce–Ce interactions are added, a quantitative, but not a qualitative change in the shape is observed. Only if the Fe–Ce interactions are considered (with or without Ce–Ce interactions), the local minimum in the heat capacity around 200 K is observed. It is apparently an artifact of $l_{max} = 2$, underlying the choice $l_{max} = 3$.

A major drawback of the classical Monte Carlo (cMC) approach is, however, that all these calculations show a non-vanishing heat capacity for $T \to 0$. As we have discussed for pure Fe earlier [43], this is due to the neglect of quantum effects. They are accurately accounted for in quantum Monte Carlo (QMC) calculations. To avoid computationally very expensive QMC simulations, we have applied the rescaling Monte Carlo (rMC) scheme developed by Körmann et al. [43], which approximates the required quantum corrections (qc) by the function

$$f^{qc}(\tau, S) = \frac{C_V^{QMC}(\tau, S)}{C_V^{cMC}(\tau, S)} = \left(\frac{2\tau_s/\tau}{\exp(\tau_s/\tau) - \exp(-\tau_s/\tau)} \right)^2. \quad (18)$$

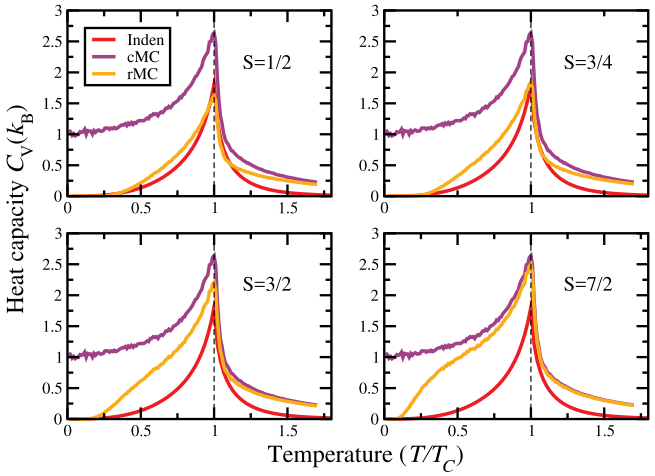

Fig. 4. Comparison of classcial Monte Carlo (cMC), rescaled Monte Carlo (rMC) and the Inden model for the heat capacities of $CeFe_2$ using different spin quantum numbers S = 1/2, 3/4, 3/2 and 7/2.

This function is multiplied with the heat capacity of the cMC result. It contains only the normalized temperature $\tau = T/T_C$ and the spin quantum number *S* as parameters, but is universal in the sense that it does not dependent on the specific material system. The scaling parameter τ_s is given as. $1/\tau_s \approx 0.54(1)S + 0.54(2)$.

The Monte Carlo results for $CeFe_2$ with different spin quantum numbers *S* are compared with the Inden model in Fig. 4. The results confirm the limited agreement of the cMC calculations with the Inden model, which is substantially improved when using the rMC approach. We note that the empirical function f^{qc} fulfills the limiting cases $f^{qc}(\tau \to \infty, S) \to 1$ and $f^{qc}(t, S \to \infty) \to 1$, meaning that the quantum approach converges to the classical solution in the limit of infinite temperature *T* or spin quantum number *S*.

The agreement between the Inden model and rMC is, however, best for low *S* values. For α-Fe the spin quantum number $S = 1.1$ has been used [43], corresponding to the *ab initio* calculated ground state magnetic moment of $m = 2.2\mu_B$. In the case of $CeFe_2$, we use again the concept of an effective magnetic moment for the ferrimagnetically coupled magnetic moments of Fe and Ce of 1.8 μ_B and -0.9 μ_B, respectively. According to Eq. (12) this yields a value $\beta = 1.46\ \mu_B$, which can in

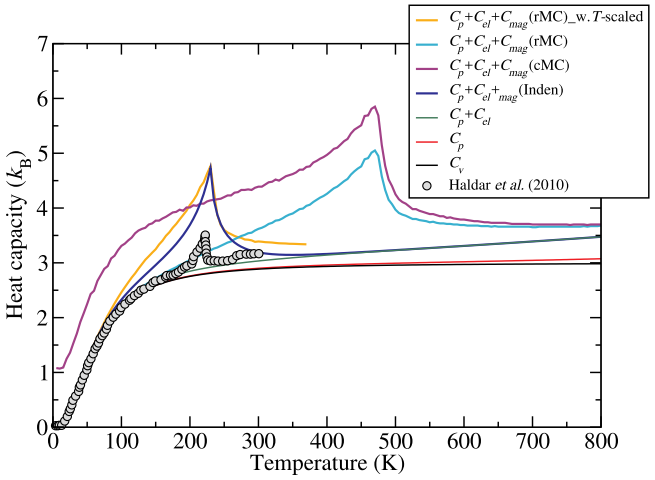

Fig. 5. Comparison of the calculated heat capacity of $CeFe_2$ with experimental results integrating the different treatments of the magnetism shown in Fig. 4. In addition the temperature of the rMC results is rescaled such that the Curie temperature matches the experimental value (orange line). The experimental data is taken form Haldar et al. [48].

good approximation be expressed as $m = (2 \cdot 1.8\,\mu_B + 0.9\,\mu_B)$. Therefore, we use S = 3/4 in the present evaluation.

Fig. 5 shows the combination of the rMC results with other entropy contributions. As can be seen, the rMC result (turquoise line) successfully cures one of the drawbacks of cMC (purple line), namely the incorrect low temperature limit resulting to a starting value of the heat capacity of ~1 k_B. A second drawback of the classical Heisenberg model underlying the Monte Carlo simulations is however, the overestimation of T_C. Therefore, we additionally rescale the temperature of the rMC heat capacities to match the experimental T_C.

The resulting heat capacity yields very good agreement with the experimental data well below and above the magnetic transition temperature. In the same way as the Inden model, however, the λ-shaped peak is overestimated by the Monte Carlo simulations as compared to experiment. Furthermore, the rMC results yield a small offset above 250 K. This indicates remaining shortcomings in the Monte Carlo approach, either related to the determination of the exchange coupling parameters, the underlying Heisenberg model, its classical solution, or finite-size effects. It further conveys the message that the conceptually simpler and more efficient Inden approach is a competitive model for the magnetic heat capacity.

Most important for our considerations are, however, the consequences for the decomposition energy shown in Fig. 1. We note that the rMC approach for the magnetic entropy of Fe and $CeFe_2$ yields a critical temperature for the decomposition, which is 40 K below the prediction of the Inden model. This is mainly due to the wrong Curie temperature of $CeFe_2$. After rescaling this temperature the differences between the Monto Carlo results and the Inden model below 800 K are very small. This indicates that the actual shape of the heat capacity of $CeFe_2$ is not very decisive for the resulting free energies, further highlighting the performance of the Inden model.

4. Effect of magnetism on finite temperature vibrational properties

While the magnetic part of the free energy F^{mag} has a strong impact on the decomposition energy F^{dec} (Fig. 1), the vibrational term F^{vib} usually forms the largest part of the total free energy in Eq. (2). Nevertheless, the magnetic state as well as finite temperature magnetic excitations also have a strong impact on the vibrational properties, as shown for pure Fe [49]. In the present work, we compute and analyze this impact on the two competing Laves phases in the Ce–Fe–Ti alloys, namely C14–Fe_2Ti and C15–$CeFe_2$.

The phonon dispersion of Fe_2Ti is calculated within DFT (Fig. 6) by considering a $1 \times 1 \times 1$ supercell containing 12 atoms. The magnetic properties of Fe_2Ti have been reported to be sensitive to deviations from stoichiometry [50]: The Fe-rich phase is ferromagnetic, while the Ti-rich Laves phase shows antiferromagnetic ordering. Here we limit ourselves to the stoichiometric case, which turns out to be antiferromagnetic and plot the corresponding phonon dispersion as black solid lines. In order to describe the lattice vibrations above the Néel temperature of 275 K [51], paramagnetic calculations are required [49]. For the complex structure of Laves phases, this would imply a huge numerical effort.

In the same spirit as in Fig. 1, we therefore use the nonmagnetic state to investigate the impact of magnetism (green dashed lines in Fig. 6). The deviation is not a trivial effect of volume expansion, since the theoretical lattice constants in the antiferromagnetic case are $a = 4.689$ Å and $c = 7.788$ Å, while the nonmagnetic calculations yields $a = 4.669$ Å and $c = 7.716$ Å. Larger lattice constants are expected to result into softer phonon modes, but opposite results are seen in Fig. 6. A comparison with the experimental phonon dispersions of Fe_2Ti is not possible, since it has not yet been reported in literature. This is likely a consequence of the complex primitive unit cell ($P6_3/mmc$#194), which has 12 atoms leading to the 36 phonon branches.

For $CeFe_2$, we also computed the phonon dispersion in a nonmagnetic and the ferrimagnetic state by considering a $1 \times 1 \times 1$ supercell containing 24 atoms. In the second case, Ce and Fe atoms have different spin moments that are aligned anti-parallel. The results are shown in Fig. 7 and compared with experimental data [52]. The latter are extended to a Born-von-Kármán model taking longitudinal and transverse forces up to the fifth nearest neighbor shell into account. Due to difficulties in finding suitable force constants [52], the Born-von-Kármán fit (triangles) deviates from the actual experimental data (dots).

For the ferrimagnetic case, we observe an overall better agreement in the phonon dispersion with experiment. Due to the lack of experimental data points, the quality of the acoustic branches in the Γ→ K direction is difficult to assess. The measurements were performed on $CeFe_2$ (lattice constant = 7.307 Å) and compared with our calculations (lattice constant of 7.092 Å for the nonmagnetic and of 7.218 Å for the ferrimagnetic case). Since in the nonmagnetic calculations the lattice constant is smaller, a stiffening of the phonon modes may be expected. However, this was not detected in our calculations. In addition to this it results in softer frequencies at the high-symmetry Γ points.

A further challenge in the DFT treatment of $CeFe_2$ are the strong

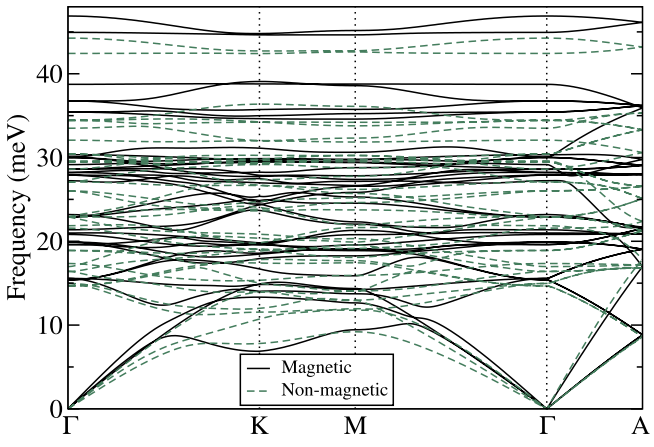

Fig. 6. Calculated phonon dispersion lines for C14–Fe_2Ti along high symmetry directions in the antiferromagnetic (black solid lines) and a nonmagnetic (green dashed lines) state.

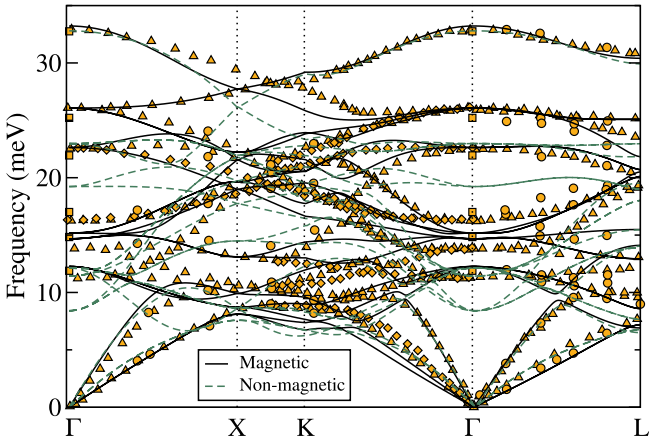

Fig. 7. Calculated phonon dispersion of C15–$CeFe_2$ compared to neutron scattering experiments performed at room temperature [52]. The calculations are performed in a ferrimagnetic (black solid lines) and a nonmagnetic (green dashed lines) state. Orange dots are experimental frequencies taken from the longitudinal configuration of the spectrometer. Triangles are phonon dispersions obtained by fitting a Born-von Kármán model to the measured data. Diamonds are branches that are not observable in the scattering plane. Squares are optical phonon frequencies determined at the centers of the Brillouin zones (Γ-point).

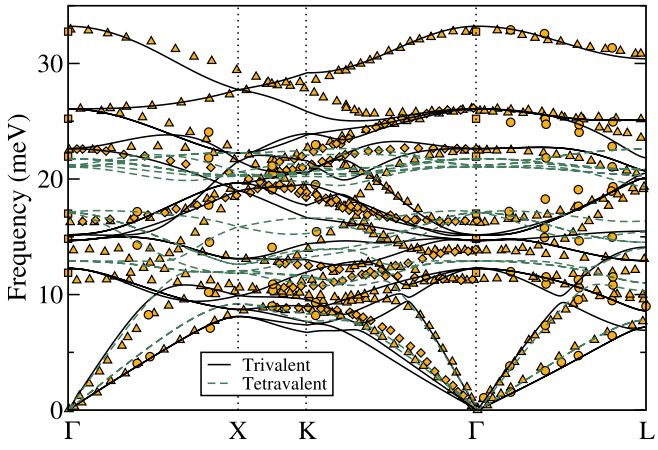

Fig. 8. Calculated phonon dispersion of $Ce^{+3}Fe_2$ (black solid line) and $Ce^{+4}Fe_2$ (green dashed line). Similar to Fig. 7, the orange symbols represent neutron scattering experiments performed at room temperature [52].

correlation effects related to the Ce-4*f* electrons. Therefore, we have calculated phonon dispersion lines for two different Ce valencies in $CeFe_2$, which are the trivalent ($Ce^{+3}Fe_2$) and the tetravalent ($Ce^{+4}Fe_2$) case. The comparison of calculated and experimental data is shown in Fig. 8. In case of the trivalent treatment, the employed potential has a $4f^1$ configuration, where the *f*-electron is treated in the valence. In case of the tetravalent configuration the *f*-electron is treated in the core. We observe dramatic deviations in the phonon spectrum due to the difference in the valency treatment, in particular for the higher frequency optical branches.

The two approaches also result in large differences in the lattice constants, which are 7.218 Å (trivalent) and 7.526 Å (tetravalent). Thus, the trivalent $CeFe_2$ is expected to agree better with experiment, since the experimental lattice constant is 7.307 Å. This expectation is confirmed by the good agreement in the optical branches. However, some of the acoustic branches are too soft. The tetravalent treatment shows better agreement with the acoustic phonon modes, but fails completely for the optical branches. The reason of such a large discrepancy may be the absence of the 4*f*-3*d* interaction in this formalism. The impact of such deviations in the phonon dispersion based on the valency treatment on the total free energy and therefore the stability of the hard-magnetic phase is subject to further investigations.

5. Sensitivity analysis for the inden model

As discussed in Sec. III, the physics of compounds containing RE elements as well as the treatment of the *f*-electron valency are challenges for KKR and MC calculations. Remarkably, the empirical Inden model provides heat capacities with comparable accuracy, though the method was originally designed for much simpler, unary ferromagnets such as Fe, Co, and Ni. To understand this universal applicability of the Inden model, it is necessary, to study its performance for different permanent magnetic materials more systematically. To do this, we consider $CeFe_{11}Ti$ and $Nd_2Fe_{14}B$, in which *f*-electrons have itinerant and localized character, respectively. We note that the established treatment of both phases in the framework of DFT differs: In the phase $CeFe_{11}Ti$, the 4*f* electrons are strongly hybridized with the 3*d* electrons, making the application of conventional DFT feasible. In the case of $Nd_2Fe_{14}B$, however, the localization of the 4*f* electrons requires the application of correction schemes such as DFT + *U* [27].

Fig. 9(a) shows the *ab initio* computed heat capacity for $CeFe_{11}Ti$ together with available experimental data reported by Kavakbasi [53]. The experimental sample had a purity of 98.82% $CeFe_{11}Ti$, according to a X-ray diffraction (XRD) analysis. Experiments were performed in a temperature range of 0–395 K. An excellent agreement between

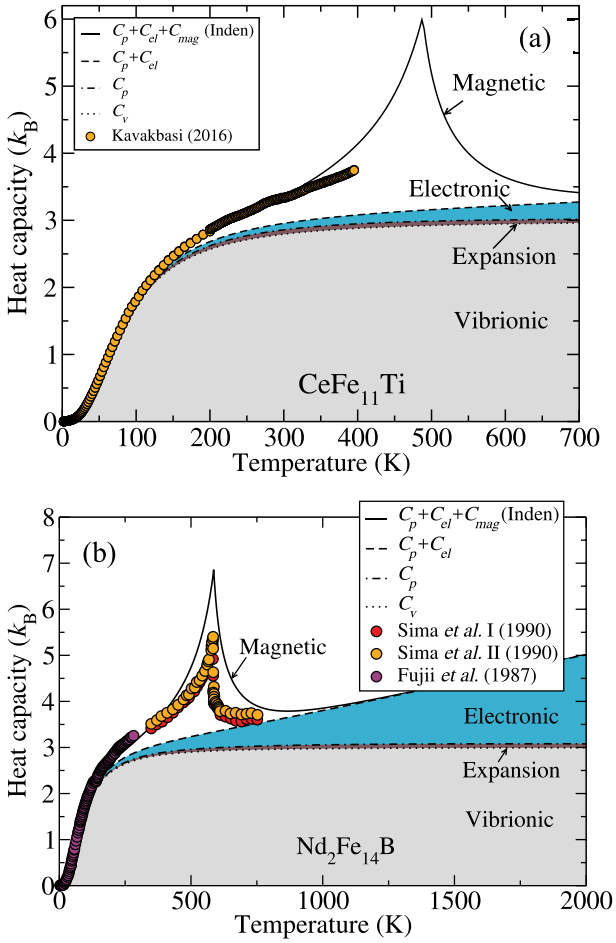

Fig. 9. Calculated heat capacity of $CeFe_{11}Ti$ and $Nd_2Fe_{14}B$, separating the different free-energy contributions in Eq. (2). The theoretical results are compared with experimental data obtained by Kavakbasi [53] for $CeFe_{11}Ti$ and Sima et al. [54] and Fuji et al. [55] for $Nd_2Fe_{14}B$.

simulations and experiment was found up to room temperature. Since heat capacity data close to the magnetic transition are missing, evaluating the accuracy of the Inden model to predict the λ-shaped peak is not possible. Since theoretical curve in Fig. 9 shows a pronounced peak, it is important to evaluate the dependence of its shape on the parameters in the Inden model.

Fig. 9(b) gives the calculated heat capacity of the presently best hard magnet $Nd_2Fe_{14}B$ together with corresponding experimental data. Fujii et al. [55] measured the heat capacity up to room temperature and reported a spin-reorientation and a small bump at $T = 135$ K. Sima et al. [54] performed additional measurements in the temperature range between 350 to 780 K.

Our *ab initio* calculations of $Nd_2Fe_{14}B$ employed DFT + *U*, to account for the localization of the *f*-electrons. In order to obtain an appropriate choice for the Hubbard *U*, we have screened *U* values between 1 and 10 eV. $U = 6$ eV yields the best description of the magnetic moments of the Nd atomic sites (the Hubbard *U* is only applied to this site) and of spectroscopic properties. A good agreement between the theoretical and experimental values for the heat capacity is observed good until ~500 K. Beyond this temperature the magnetic contribution slightly overestimates the experimental heat capacity. Given the empirical nature of the Inden model, the λ-shaped peak is very well described.

Since experimental data for the heat capacity of $Nd_2Fe_{14}B$ are available for larger temperatures ranges that contain the magnetic transition, we will focus the upcoming discussion on this compound. To resolve the remaining differences, we analyze the sensitivity of the heat

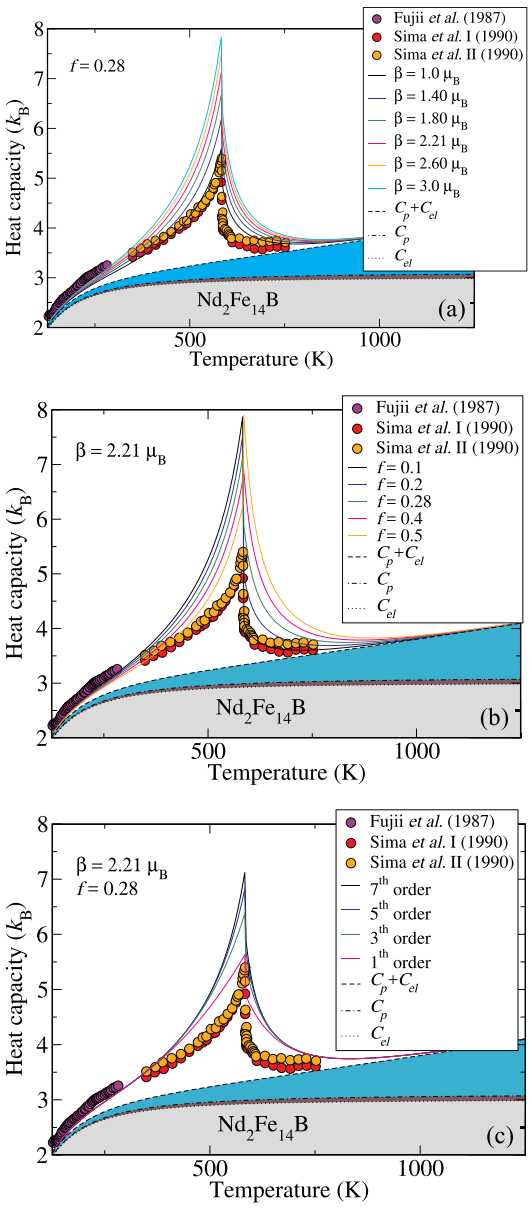

Fig. 10. Calculated heat capacities of $Nd_2Fe_{14}B$ for different set of parameters in the mathematical formulation of the Inden model. Sensitivity of the mean magnetic moment β, structure parameter *f* and the order of Taylor expansion is given from (a) to (c), respectively. The separation of the heat capacity in different free-energy contributions in Eq. (2) is designated as in Fig. 9. Theoretical results are compared with the experimental works Sima et al. [54] and Fuji et al. [55] for $Nd_2Fe_{14}B$. Since the agreement is perfect at low temperatures, figures are started with 125 K and 2 k_B heat capacity for better comparison.

capacity on the parameters in the Inden model: the mean magnetic moment β, the structural parameter *f*, and the order of the Taylor expansion. The results are plotted in Fig. 10. The original choice for the Inden model used in Fig. 9 is $f = 0.28$, $\beta = 2.21\ \mu_B$ and the 7th order in the Taylor expansion. The choice of the mean magnetic moment perfectly agrees to the experimental value, 2.18 μ_B, that has been measured at 4.2 K by Givord et al. [56].

The change in the heat capacity, if *f* is kept constant as 0.28 and β is gradually changed from 1 μ_B to 3 μ_B is shown in Fig. 10(a). The modification of the qualitative shape in the LRO and SRO part of the λ peak is significant. The best agreement with experiment is achieved for $\beta = 1\mu_B$. Therefore, the overestimation of the heat capacity by the initial setup ($\beta = 2.21\ \mu_B$) can be a consequence of determining the *ab initio* based magnetic moments at $T = 0$ K. In reality, longitudinal fluctuations reduce the magnetic moments at finite temperatures, an effect that is also missing in the MC simulations presented in Chap. III.

In order to test whether the improvement is merely a mathematical coincidence we tested alternative parameter sets. We therefore set $\beta = 2.21\ \mu_B$ and vary the *f* parameter from 0.1 to 0.5. As can be seen in Fig. 10(b), the parameter *f* mainly serves as a scaling factor, resulting however into two opposite trends: While the reduction of *f* clearly improves the agreement of the heat capacity above T_C, the opposite is the case below T_C. The value $f = 0.1$ best describes the SRO part. In contrast, a value of *f* above 0.5 is required to achieve a reasonable description of the LRO part of the peak.

Following the discussion in Sec. II we have also tested the dependence of the heat capacity on the Taylor expansion (given in Eq. (11)), while setting $\beta = 2.21\ \mu_B$ and $f = 0.28$. By construction, this dependence only changes absolute values and slopes of the heat capacity close to the transition temperature. We start with an expression of the heat capacity that contains up to 7th order in temperature as proposed by Chen and Sundman [40]. As can be seen in Fig. 10(c) the consideration of the 7th and even 5th order term has negligible impact on the shape of the λ peak. While the reduction to lower orders yields a quantitatively better agreement with experiment, the shape of the λ-peak gets worse. Hence, an improved description of the heat capacity can only be achieved with the initial values for *f* and the power of the Taylor expansion and an adaptation of the parameter β for the magnetic moment.

6. Conclusion

In conclusion, we systematically studied how magnetism impacts the finite temperature phase stability of Ce–Fe–Ti alloys. Only when including magentic contributions, our free energy calculations are able to accurately reproduce the competition between the desired hard magnetic phase $CeFe_{11}Ti$ and the parasitic Laves phase $CeFe_2$ in the microstructure of these materials [22]. Based on this insight, the *ab initio* methodology to compute the magnetic free energy has been analyzed in detail.

A central quantity studied in this paper is the critical temperature at which the phase $CeFe_{11}Ti$ decomposes into the Laves phases $CeFe_2$, Fe_2Ti and pure Fe. The correct treatment of the magnetic entropy is found to be decisive for this purpose, because its neglect yields a critical temperature that is by far too high. Using the magnetic model originally suggested by Gerhard Inden, however, allowed us to achieve in this study free energies of the involved phases that accurately reproduce this critical quantity.

A more rigorous but computationally much more expensive approach using Monte Carlo simulations for an *ab initio* magnetic model Hamiltonian was found to be not superior: When taking the experimental heat capacity as a benchmark a similar performance has been achieved. Some of the challenges we had to resolve to obtain an accurate description are the treatment of *f*-electrons and the valency of Ce in the KKR method and the inclusion of quantum corrections to the Monte Carlo simulations. For the latter case, we demonstrated that the rescaled Monte Carlo (rMC) approach, which has previously been developed for unary materials, works also well for these compounds. Nevertheless, the necessary approximation of the underlying Heisenberg Hamiltonian and the omission of longitudinal fluctuations are possible reasons for the remaining discrepancies and the limited performance of this approach.

Our investigations reveal that the Inden model tends to overestimate the λ-shaped peak in the heat capacity associated with the magnetic phase transition. For a deeper analysis we have considered the example of the hard magnetic material $Nd_2Fe_{14}B$. This alloy is chemically and structurally similar to $CeFe_{11}Ti$, but has been calorimetrically investigated over the full temperature window including the magnetic transition. We have investigated the sensitivity of the heat capacity on the parameters of the Inden model and have revealed that a reduction of the

mean magnetic moment β substantially improves the agreement between theory and experiment. The physical interpretation of this phenomenon is a reduction of the local magnetic moment due to longitudinal fluctuations close to the magnetic transition temperature. In contrast to previous studies, the order of the Taylor expansion in the magnetic model of the Gibbs energy turns out to be of comparatively small importance.

We note that the magnetic entropy is not the largest contribution to the free energies determining the decomposition temperature. Rather, vibrational contributions dominate. Based on a detailed comparison with the heat capacity data, the quasi-harmonic approximation for the phonon excitations was found to provide a sufficiently accurate description of lattice vibrations. A comparison with the experimentally available phonon dispersions, however, revealed the importance of the correct choice of the magnetic state of the material. This impact of magnetism on phonons has been analyzed with focus on Fe_2Ti and $CeFe_2$. An extension of the current approach to the paramagnetic state above the Curie temperature is, therefore, required and subject to further investigations.

Declaration of competing interest

The authors declare that they have no known competing financial interests or personal relationships that could have appeared to influence the work reported in this paper.

Acknowledgements

The authors would like to thank Prof Gerhard Inden for various exiting discussions on thermodynamic models for alloys and compounds. We very much appreciate the tremendous contributions he has made to our community. His pioneering ideas to treat magnetism in Fe-based materials had and will continue to have a strong impact on steel research as performed at the Max-Planck-Institut für Eisenforschung. Our project on rare-earth based alloys for hard-magnetic applications: temperature and pressure dependent phase stabilities (RE-MAP) is supported by Deutsche Forschungsgemeinschaft (DFG, Grant No. HI 1300/14-1) and Agence nationale de la recherche (ANR, Grant No. ANR-16-CE92- 0029).

Appendix A. Supplementary data

Supplementary data related to this article can be found at https://doi.org/10.1016/j.calphad.2019.101731.

References

[1] S. Sugimoto, J. Phys. D Appl. Phys. 44 (2011), 064001.
[2] J.J. Croat, J.F. Herbst, R.W. Lee, F.E. Pinkerton, J. Appl. Phys. 55 (1984) 2078.
[3] M. Sagawa, S. Fujimura, N. Togawa, H. Yamamoto, Y. Matsuura, J. Appl. Phys. 55 (1984) 2083.
[4] K.P. Skokov, O. Gutfleisch, Scr. Mater. 154 (2018) 289.
[5] I. Poenaru, A. Lixandru, S. Riegg, B. Fayyazi, A. Taubel, K. Güth, R. Gauß, O. Gutfleisch, J. Magn. Magn. Mater. 478 (2019) 198.
[6] N. Drebov, A. Martinez-Limia, L. Kunz, A. Gola, T. Shigematsu, T. Eckl, P. Gumbsch, C. Elsässer, New J. Phys. 15 (2013), 125023.
[7] W. Körner, G. Krugel, C. Elsässer, Sci. Rep. 6 (2016) 24686.
[8] L. Nordstroem, B. Johansson, M.S.S. Brooks, J. Phys. Condens. Matter 5 (1993) 7859.
[9] A. Alam, M. Khan, R.W. McCallum, D.D. Johnson, Appl. Phys. Lett. 102 (2013), 042402.
[10] A. Alam, D.D. Johnson, Phys. Rev. B Condens. Matter Mater. Phys. 89 (2014) 12, arXiv:arXiv:1311.0962v1.
[11] L. Ke, D.D. Johnson, Phys. Rev. B 94 (2016), 024423.
[12] A. Debernardi, M. Alouani, H. Dreyssé, Phys. Rev. B Condens. Matter Mater. Phys. 63 (2001) 1.
[13] P. Souvatzis, O. Eriksson, Phys. Rev. B 77 (2008), 024110.
[14] Y.-Y. Chuang, R. Schmid, Y.A. Chang, Metall. Trans. A 16 (1985) 153.
[15] G. Inden, in: Proceedings of CALPHAD V, Max-Planck Inst. Eisenforschung, Düsseldorf, 1976, pp. 1–13.
[16] G. Inden, Phys. B+C 103 (1981) 82.
[17] J. Korringa, Physica 13 (1947) 392.
[18] W. Kohn, N. Rostoker, Phys. Rev. 94 (1954) 1111.
[19] A.I. Liechtenstein, M.I. Katsnelson, V.A. Gubanov, J. Phys. F Met. Phys. 14 (1984) L125.
[20] M. Ležaić, P. Mavropoulos, S. Blügel, Appl. Phys. Lett. 90 (2007), 082504.
[21] A.W. Sandvik, J. Kurkijarvi, Phys. Rev. B 43 (1991) 5950.
[22] H.I. Sözen, S. Ener, F. Maccari, K.P. Skokov, O. Gutfleisch, F. Körmann, J. Neugebauer, T. Hickel, Phys. Rev. Mater. 3 (2019), 084407.
[23] G. Kresse, J. Hafner, Phys. Rev. B 47 (1993) 558.
[24] G. Kresse, J. Furthmüller, Phys. Rev. B 54 (1996), 11169.
[25] P.E. Blöchl, Phys. Rev. B 50 (1994), 17953.
[26] J.P. Perdew, K. Burke, M. Ernzerhof, Phys. Rev. Lett. 77 (1996) 3865.
[27] S.L. Dudarev, S.Y. Savrasov, C.J. Humphreys, A.P. Sutton, Phys. Rev. B 57 (1998) 1505.
[28] T. Hickel, B. Grabowski, F. Körmann, J. Neugebauer, J. Phys. Condens. Matter 24 (2012), 053202.
[29] N.D. Mermin, Phys. Rev. 137 (1965), A1441.
[30] X. Zhang, B. Grabowski, F. Körmann, C. Freysoldt, J. Neugebauer, Phys. Rev. B 95 (2017) 165126.
[31] K. Parlinski, Z. Li, Y. Kawazoe, Phys. Rev. Lett. 78 (1997) 4063.
[32] B. Grabowski, T. Hickel, J. Neugebauer, Phys. Rev. B 76 (2007), 024309.
[33] http://www.sphinxlib.de.
[34] S. Boeck, Development and Application of the S/PHI/nX Library, Sudwestdeutscher Verlag fur Hochschulschriften, 2009.
[35] M. Methfessel, A.T. Paxton, Phys. Rev. B 40 (1989) 3616.
[36] D.C. Wallace, Thermodynamics of Crystals, Dover, New York, 1998.
[37] L. Zhou, F. Körmann, D. Holec, M. Bartosik, B. Grabowski, J. Neugebauer, P. H. Mayrhofer, Phys. Rev. B Condens. Matter Mater. Phys. 90 (2014), 184102.
[38] F. Körmann, A.A.H. Breidi, S.L. Dudarev, N. Dupin, G. Ghosh, T. Hickel, P. Korzhavyi, J.A. Muñoz, I. Ohnuma, Phys. Status Solidi B. Basic. Res. 251 (2014) 53.
[39] M. Hillert, M. Jarl, Calphad 2 (1978) 227.
[40] Q. Chen, B. Sundman, J. Phase Equilibria 22 (2001) 631.
[41] W. Xiong, Q. Chen, P.A. Korzhavyi, M. Selleby, Calphad Comput. Coupling Phase Diagrams Thermochem. 39 (2012) 11.
[42] H. Sawada, K. Kawakami, F. Koermann, B. Grabowski, T. Hickel, J. Neugebauer, Acta Mater. 102 (2016) 241.
[43] F. Körmann, A. Dick, T. Hickel, J. Neugebauer, Phys. Rev. B 81 (2010), 134425.
[44] H. Akai, J. Phys. Condens. Matter 1 (1989) 8045.
[45] H. Akai, P.H. Dederichs, Phys. Rev. B 47 (1993) 8739.
[46] M. Schröter, H. Ebert, H. Akai, P. Entel, E. Hoffmann, G.G. Reddy, Phys. Rev. B 52 (1995) 188.
[47] A.I. Liechtenstein, M.I. Katsnelson, V.P. Antropov, V.A. Gubanov, J. Magn. Magn. Mater. 67 (1987) 65.
[48] A. Haldar, K.G. Suresh, A.K. Nigam, J. Phys. D Appl. Phys. 43 (2010), 285004.
[49] F. Körmann, B. Grabowski, B. Dutta, T. Hickel, L. Mauger, B. Fultz, J. Neugebauer, Phys. Rev. Lett. 113 (2014) 1.
[50] T. Nakamichi, J. Phys. Soc. Japan 25 (1968) 1189.
[51] A.A. Novakova, O.V. Agladze, S.V. Sveshnikov, B.P. Tarasov, Nanostructured Mater. 10 (1998) 365.
[52] L. Paolasini, B. Hennion, A. Panchula, K. Myers, P. Canfield, Phys. Rev. B 58 (1998), 12125.
[53] B. T. Kavakbasi, (To be submitted) (2019).
[54] V. Sima, P. Haasen, J. Wecker, IEEE Trans. Magn. 26 (1990) 2610.
[55] H. Fujii, H. Nagata, Y. Uwatoko, T. Okamoto, J. Magn. Magn. Mater. 70 (1987) 331.
[56] D. Givord, H. Li, R. Perrier de la Bâthie, Solid State Commun. 51 (1984) 857.